JOURNAL OF GEOPHYSICAL RESEARCH, VOL. 103, NO. D13, PAGES 16,385–16,396, JULY 20, 1998

A study of new particle formation and growth involving biogenic and trace gas species measured during ACE 1

Rodney J. Weber,[1] Peter H. McMurry,[2] Lee Mauldin,[3] David J. Tanner,[3] Fred L. Eisele,[3,4] Fred J. Brechtel,[5] Sonia M. Kreidenweis[5], Gregory L. Kok,[6] Richard D. Schillawski,[6] and Darrel Baumgardner[6]

Abstract. Measurements are presented of ambient nanoparticle distributions (2.7 to 10 nm diameter) in regions of high biogenic emissions encountered during the First Aerosol Characterization Experiment (ACE 1), November 15 to December 14, 1995. Large numbers of newly formed nanoparticles were observed directly downwind of penguin colonies on Macquarie Island (54.5°S, 159.0°W). In these regions, nanoparticle concentrations were also correlated with sulfuric acid ($H_2SO_{4(g)}$) gas concentrations. The measurements show that biogenic species, possibly ammonia (NH_3), either by itself or with H_2SO_4, nucleated to form new particles at rates much higher than bimolecular H_2SO_4/H_2O nucleation. Nanoparticle distributions evolved as air was advected away from the island showing clear evidence of growth of the newly formed particles. Observed growth rates were in the range of 2 to 5 nm h^{-1} and were about a factor of 4 to 17 times higher than the growth by condensing $H_2SO_{4(g)}$ and associated water. The cause for fast growth of the newly formed particles is unknown.

1. Background

Concentrations of fine tropospheric aerosol particles (~20 nm-1 μm diameter) are influenced by processes such as nucleation, growth by condensing vapors, coagulation, and wet and dry deposition [e.g., *Bates et al.*, this issue (a)]. Because these particles are thought to play an important role in global climate, there is a significant effort to understand the processes which affect their concentrations [e.g., *Charlson et al.*, 1987]. Some of these processes, such as the formation of new particles by nucleation of gas phase species and growth of newly formed particles, are poorly understood, primarily due to a lack of understanding of which gas phase species participate. Models for aerosol formation in the remote troposphere often assume that new fine particles are produced in situ by homogenous bimolecular nucleation of sulfuric acid ($H_2SO_{4(g)}$) and water ($H_2O_{(g)}$) vapor, and that newly formed particles grow by condensation of these gases [e.g., *Hegg et al.*, 1990; *Kreidenweis et al.*, 1991; *Hegg et al.*, 1992; *Lin et al.*, 1992; *Raes et al.*, 1992; *Easter and Peters*, 1994; *Perry and Hobbs*, 1994; *Russell et al.*, 1994; *Raes*, 1995].

Our previous work has suggested that in the remote troposphere, both particle nucleation rates and nanoparticle (referred to here as particles between ~3 and 10 nm diameter) growth rates can, in certain locations, be much higher than those predicted for the H_2SO_4/H_2O system [*Weber et al.*, 1995, 1996, 1997a]. Measurements at both Mauna Loa, Hawaii, and Idaho Hill, Colorado, showed that $H_2SO_{4(g)}$ was highly correlated with nanoparticle concentrations which were likely formed by recent nucleation. At both sites, evidence for nucleation was observed at $H_2SO_{4(g)}$ concentrations in the range of 10^6 to 10^7 molecules cm^{-3}, too low for new particle formation by H_2SO_4/H_2O nucleation for the temperatures and relative humidities at these sites. Moreover, in contrast to the H_2SO_4/H_2O system, observed nucleation rates did not appear to be highly sensitive to either $H_2SO_{4(g)}$ or $H_2O_{(g)}$ concentrations. Our data suggested that particle formation rates were proportional to $[H_2SO_{4(g)}]^2$ not to powers of 8 to 12 as predicted for H_2SO_4/H_2O nucleation. We speculated that these differences could be due to the participation of other species and have focused specifically on ammonia (NH_3). Ammonia is present throughout the remote troposphere and efficiently reacts with sulfuric acid particles [*Huntzicker et al.*, 1980; *McMurry et al.*, 1983]. Moreover, recent measurements show that the vapor pressure of $H_2SO_{4(g)}$ over such particles is reduced by orders of magnitude compared to that of H_2SO_4 droplets [*Marti et al.*, 1997a]. We speculate that additional trace gas species (e.g., $NH_{3(g)}$) reduce the vapor pressures of the participating species, thereby permitting nucleation to occur at much lower sulfuric acid partial pressures. We have not been able to show that $NH_{3(g)}$ participates in particle formation. We report here, however, on new evidence of nucleation in regions where biogenic $NH_{3(g)}$ levels are expected to be high.

Our earlier work at a forested site in the Colorado Rocky Mountains [*Weber et al.*, 1997a] has also shown that nanoparticle growth rates can be ~5 to 10 times higher than growth of H_2SO_4 and associated water. Although participation of $NH_{3(g)}$ may significantly alter nucleation rates, it should not

[1] Environmental Chemistry Division, Brookhaven National Laboratory, Upton, New York.
[2] Particle Technology Laboratory, Department of Mechanical Engineering, University of Minnesota, Minneapolis.
[3] Atmospheric Chemistry Division, National Center for Atmospheric Research, Boulder, Colorado.
[4] Georgia Tech Research Institute, Georgia Institute of Technology, Atlanta.
[5] Department of Atmospheric Science, Colorado State University, Fort Collins.
[6] Research Aviation Facility, National Center for Atmospheric Research, Boulder, Colorado.

Paper number 97JD02465
0148-0227/98/97JD-02465$09.00

account for the much higher growth rates. It is known that naturally occurring organic species, such as terpenes, can nucleate to form new particles [*Tyndall*, 1868; *Went*, 1960; *Went*, 1966]. We speculated that in Colorado, nucleation involved reactions between $H_2SO_4/NH_3/H_2O$ (and possibly other species), while the rapid growth was due to condensation of secondary organics [*Marti et al.*, 1997b]. Recent work by *Kerminen et al.* [1997] has also suggested that participation of nitric (HNO_3) and/or hydrochloric acid (HCl) could greatly enhance growth rates of newly formed $H_2SO_4/NH_3/H_2O$ particles once a certain size has been achieved.

As part of the first Aerosol Characterization Experiment (ACE 1), various trace gas species and nanoparticle spectra were measured from the National Center for Atmospheric Research (NCAR) C-130 aircraft. Measurements were made over the remote Pacific from October 31 to December 23, 1995. On the basis of our measurements of nanoparticle spectra, we observed evidence for nucleation in regions of cloud outflow [e.g., *Clarke et al.*, this issue], in thin layers above temperature inversions, and downwind of penguin colonies on Macquarie Island. In this paper we focus on the measurements of new particle formation and nanoparticle growth downwind of Macquarie Island. Although conditions which made nucleation possible in these regions are not typical of the remote atmosphere, the densely populated and highly localized penguin colonies on Macquarie Island are likely a significant sources of $NH_{3(g)}$ [*Lindeboom*, 1984; *Mizutani and Wada*, 1988] making it an ideal location to test our hypothesis that $NH_{3(g)}$ may participate in new particle formation.

2. Macquarie Island

Macquarie Island, Australia, is a small subantarctic island (54.5°S, 159.0°W) approximately 34 km long and 5.5 km wide. The island essentially points in a north-south direction (see, for example, Figure 5). Formed by uplifting, the island consists of a rolling plateau approximately 200 m above sea level surrounded on the perimeter by a low coastal fringe. Small peaks are scattered throughout the plateau with highest elevations approximately 400 m above sea level (asl). The island is located in latitudes characterized by persistent strong westerly winds. Average near-surface wind speeds are 6-7 m s^{-1} (22-25 km h^{-1}).

Because of its isolation and unique wildlife, Macquarie Island was declared a wildlife sanctuary in 1933. The only human inhabitants on the island operate an Australian National Antarctic Research Expeditions (ANARE) Station located at the northern tip of the island. The unique feature of Macquarie Island is the wildlife. It has one of the largest populations of sea birds in the world. Penguin colonies are dispersed throughout the island; however, particularly large colonies are situated on the east coast (see Figure 5). For example, a colony of royal penguins at Hurd Point covering approximately 67,000 m^2 consists of the order of 10^5 birds. Large colonies of king and royal penguins are also located at Lusitania and Sandy Bay, respectively. A colony of royal penguins is also located at the Nuggets which in 1984 was estimated at 20,000 birds. Penguins populate the island from mid-September to mid-February to lay eggs and fledge chicks and were present during our flight on November 27, 1995. A detailed description of the island environment and biology is given by *Selkirk et al.* [1990].

3. Instrumentation

The C-130 carried a suite of gas phase and aerosol measurement instrumentation. In addition, aerosol measurements were made at the ANARE station on Macquarie Island. Descriptions of many of these instruments can be found in other reports in this issue (see *Brechtel et al.* [this issue] for a description of ground-based aerosol measurements). Meteorological and related data were provided by both the ground station and the C-130.

Ground-based aerosol instrumentation included a TSI 3025 Ultrafine Condensation Particle Counter (UCPC; TSI Inc., St. Paul, Minnesota), a TSI 3010 CPC, and a differential mobility spectrometer to measure 20 to 500 nm particle size distributions. The 3025 and 3010 measure all particles larger than roughly 3 and 12 nm, respectively, and, by difference, provide an estimate of the concentration of nanoparticles (3 to 12 nm).

Aircraft instrumentation for measuring gas phase species and aerosol particles pertinent to this study were similar to those deployed in our earlier studies but modified for aircraft sampling. Total sulfuric acid vapor concentrations (free acid plus hydrated acid) were measured using a unique chemical ionization mass spectrometer [*Eisele and Tanner*, 1993]. Nanoparticle concentrations were measured with a white-light UCPC [*Stolzenburg and McMurry*, 1991] equipped for pulse height analysis. Both $H_2SO_{4(g)}$ and nanoparticles were sampled directly from inlets near the front of the aircraft but on opposite sides. Sulfuric acid was sampled with a custom designed inlet to minimize losses and to exclude liquid water. Measurements of nanoparticles were made from the community aerosol inlet [see *Bates et al.*, this issue (b)].

Ambient air for nanoparticle sampling was transported to the UCPC via a 1 inch diameter copper tube at a flow rate of 30 L min^{-1} through a distance of approximately 5 m. Care was taken to minimize transport losses of nanoparticles by extracting sample air from the centerline of tubing, and appropriate flow rates were chosen to maintain laminar flow. We estimate sampling and transport loses of 3 nm particles to be of the order of 50%. No corrections for losses were made. The measurement intervals for $H_2SO_{4(g)}$ and nanoparticles were 30 and 60 s, respectively. Thus, at a typical airspeed of 100 m s^{-1}, measured $H_2SO_{4(g)}$ and nanoparticle concentrations represent an average over distances of ~3 and 6 km, respectively. To reduce sampling losses by diffusional deposition and at the expense of spatial resolution, we chose to sample nanoparticles directly rather than to use a bag sampling system.

Nanoparticle concentrations were determined from the UCPC photo detector pulse heights. In our previous field studies [*Weber et al.*, 1995, 1997a], we used measured UCPC pulse heights to estimate the concentrations of nominally 3 to 4 nm particles (referred to in this paper as $\tilde{N}(3\text{-}4)$). This technique provides only an estimate of the concentrations of particles between ~3 and 4 nm, but its high sensitivity and narrow size range make it the best method for identifying regions of new particle formation. For example, for the sampling conditions in this study, a measurement of $\tilde{N}(3\text{-}4)$ of 1 particle cm^{-3} has an uncertainty of ~20%. In regions of high nanoparticle concentrations, we invert UCPC pulse heights to obtain nanoparticle spectra.

We have just recently developed the technique to invert pulse height distributions to nanoparticle size distributions [*Weber et al.*, 1997b]. The inversions are performed by the algorithm

MICRON [*Wolfenbarger and Seinfeld*, 1990]. Kernel functions, which give the pulse height distribution produced by monodisperse particles of a given size, are required for these inversions and were obtained from laboratory experiments. During aircraft sampling, factors such as abrupt changes in altitude during a measurement may affect kernel functions. In this paper, we only report inverted distributions in which we have reasonable confidence. Also, since the effect of ambient pressure on UCPC counting efficiency is not well characterized, we have not accounted for counting efficiency. Thus, for sizes less than ~4 nm, the distributions should be considered a lower limit to the actual sampled distribution.

Other aircraft-based measurements of aerosol particles were made. Concentrations of particles larger than ~15 nm diameter were measured with a TSI 3760 (referred to in this paper as NCAR 3760). This instrument sampled from a forward-facing nominally isokinetic inlet located on the belly of the aircraft rather than from the community aerosol inlet. Throughout this study, in the absence of cloud droplets, CPC's sampling from the community aerosol inlet were in good agreement with the NCAR 3760 CPC indicating that there were no large biases due to our sampling strategies.

4. Flight Path in Vicinity of Macquarie Island

The measurements for this study were made on November 27, 1995, at a local time of ~1356 to 1644 (0056 to 0344 UTC) with the measurements in the immediate vicinity of the island between 1611 to 1630 local time. During this study, a high-pressure system resulted in unusually clear air of Antarctic origin. Clear conditions prevailed throughout most of the experiment, however, some clouds did appear toward the end of our measurements.

Figure 1 shows the flight path of the C-130 with respect to Macquarie Island. The aircraft position relative to the island was determined from Global Positioning System (GPS)-derived latitude and longitude. The ANARE station at the northern tip of the island was chosen as the reference point. The aircraft performed soundings and three large circles at 40, 225, and 600 m asl north of the island with only the southernmost edge of these circles in a region downwind of the island. In the final circle, extending farthest to the northeast, the aircraft approached the northern tip of the island at an altitude of ~600 m asl dropping down to ~40 m by the time we past the ANARE station and remained at this low altitude for a pass approximately 1 km off the lee shore. The aircraft turned around south of the island and then headed up the coast again, this time about 3 and 4 km off shore. During the second leg along the lee coast, the aircraft climbed from ~400 m asl at the southern tip to ~600 m asl by the time we passed the northern tip of the island.

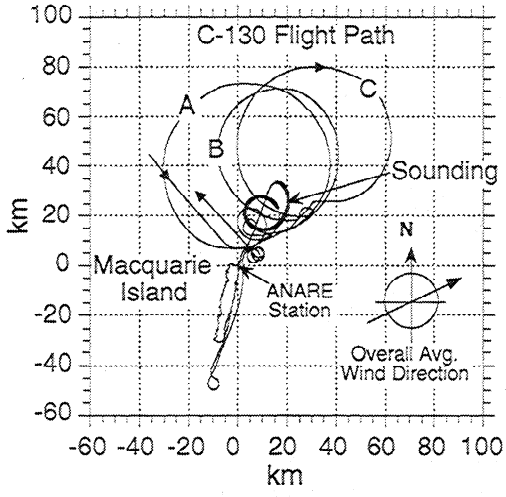

Figure 1. Flight path of aircraft relative to Macquarie Island (54.5°S, 159.0°W). GPS latitude and longitude have been converted to distances from the ground-based ANARE station at the northern tip of the island. A sounding in undisturbed air was performed north of the island.

5. Measurement Intercomparison

Aircraft and ground-based measurements can be compared during the low-altitude pass of the ANARE station just prior to the runs along the lee coast. Table 1 summarizes various meteorological and aerosol data for the aircraft sampling just north of the island and measurements recorded at the ANARE station at that time. All aircraft-based measurements have been averaged over the 60 s UCPC sample interval. The measurements on the island and C-130 agree to ~10%, as do the aircraft CPC's. None of the measurements have been corrected for sampling losses. Both measurement locations recorded similar particle concentrations and neither recorded significant levels of nanoparticles at this time.

During the overall time for this study, the aerosol concentrations recorded at the ANARE station remained steady and showed no evidence of significant numbers of nanoparticles. Average concentrations of particles larger than 3 and 12 nm were 437 and 452 cm^{-3} respectively, each with a standard deviation of less than 6%. The ground-based fine particle size distributions, shown in Figure 2, also indicate no evidence of particle formation. Figure 2 shows that there were significantly fewer particles smaller than 30 nm present at the time of the C-130 overflight than typically observed during the ACE 1 study. Overall, the ANARE measurements show no evidence of particle formation in boundary layer air reaching Macquarie Island.

Table 1. Comparison of Meteorological and Aerosol Particle Measurements at the Ground-Based Station ANARE Located at the Northern Tip of Macquarie Island and the C-130 During a Low-Altitude Pass

	ANARE Station	C-130 Sample 229
Local time	1405-1415	1411-1412
T, °C	6.3	3.8
RH, %	47	59
Wind speed, m s^{-1}	7	8.4
Wind direction., degrees from N	245	243
Altitude, m	5	67
CN, D_p>3 nm, cm^{-3}	501	558
CN, D_p>12 or 15 nm, cm^{-3}	519 (D_p>12)	553 (D_p>15)
$\tilde{N}$(3-4), cm^{-3}	—	0.1

Figure 5 shows the position of the aircraft relative to the ANARE station (e.g., black band identified by sample number 229).

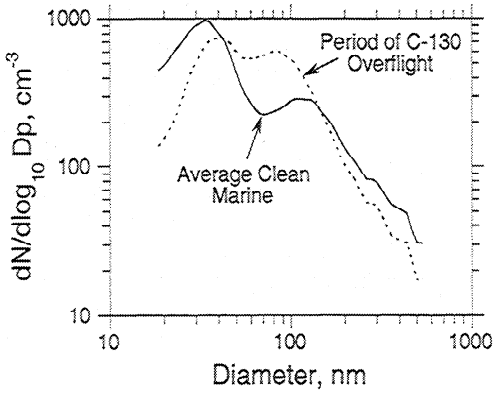

Figure 2. Average size distributions measured at the ground-based ANARE station during clean marine conditions during ACE 1 (solid line) and during the C-130 overflight (dotted line).

6. Climatology in the Vicinity of Macquarie Island

A sounding performed north of the island (shown in Figure 1) allowed characterization of the undisturbed atmosphere in the vicinity of Macquarie Island. Figure 3 shows the variations of temperature, water mixing ratio, wind direction, and wind speed with altitude north of the island. The temperature profile shows an inversion at approximately 550 m asl. Also plotted with the temperature profile is the dry adiabatic lapse rate (-1°C/102 m). The actual lapse rate is nearly identical to the dry adiabatic lapse rate indicating the atmospheric stability was neutral. The inversion also delineates the much dryer air above from the moist air of the boundary layer (Figure 3b). Figure 3c shows that the wind speed just north of the island was fairly uniform below the inversion with an average velocity of 8.3 m s^{-1}. Wind speeds increased to between 10 and 11 m s^{-1} above the inversion. There was also significant wind shear at the inversion (Figure 3d). The surface wind direction was essentially from the west (270° from north) with an increasing southerly component with increasing altitude. Above the inversion the wind was essentially from the southwest (225° from north).

Also shown as dotted lines on each plot in Figure 3 are the profiles recorded just downwind of Macquarie Island. These data are from the aircraft climb on the second leg moving from the southern to northern tip of the island at about 3 to 4 km off shore. Only data downwind of the island are shown. Compared to undisturbed air, the variation in water concentration downwind of the island shows that island-induced turbulence caused mixing of dryer and warmer air from above into the upper levels of the boundary layer. Wind speeds in this region remained similar but dropped off just above the inversion (Figure 3c), and the island tended to straighten out the wind to a more westerly direction in its wake (Figure 3d).

Figure 4 shows the variation of $H_2SO_{4(g)}$ with altitude north of the island and also along the lee coast. In undisturbed air, the $H_2SO_{4(g)}$ concentrations in the boundary layer were uniform with altitude with an average concentration of 2.8×10^6 cm^{-3}. Above the inversion the levels rose rapidly, and in the region of 800 to 1000 m asl, ranged from 8 to ~9.5×10^6 molecules cm^{-3}.

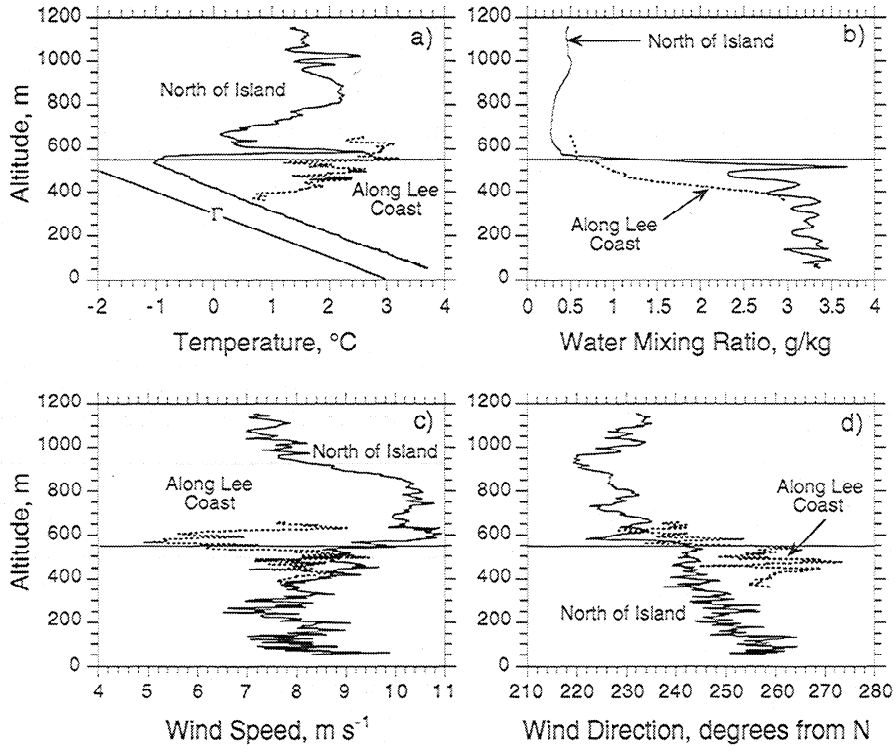

Figure 3. Structure of the atmosphere from the sounding in undisturbed air north of the island: (a) temperatures, (b) water mixing ratio, (c) wind speeds, and (d) wind direction. The profiles show a temperature inversion at ~550 m asl separating the moist boundary layer from dry air above. Figure 3a shows the dry adiabatic lapse rate (-1°C/102 m), Γ. Also shown (dotted lines) are measurements just off the lee coast of the island when the aircraft was climbing from ~400 to 560 m asl. Comparisons show that island-induced turbulence caused mixing of air in the vicinity of the inversion.

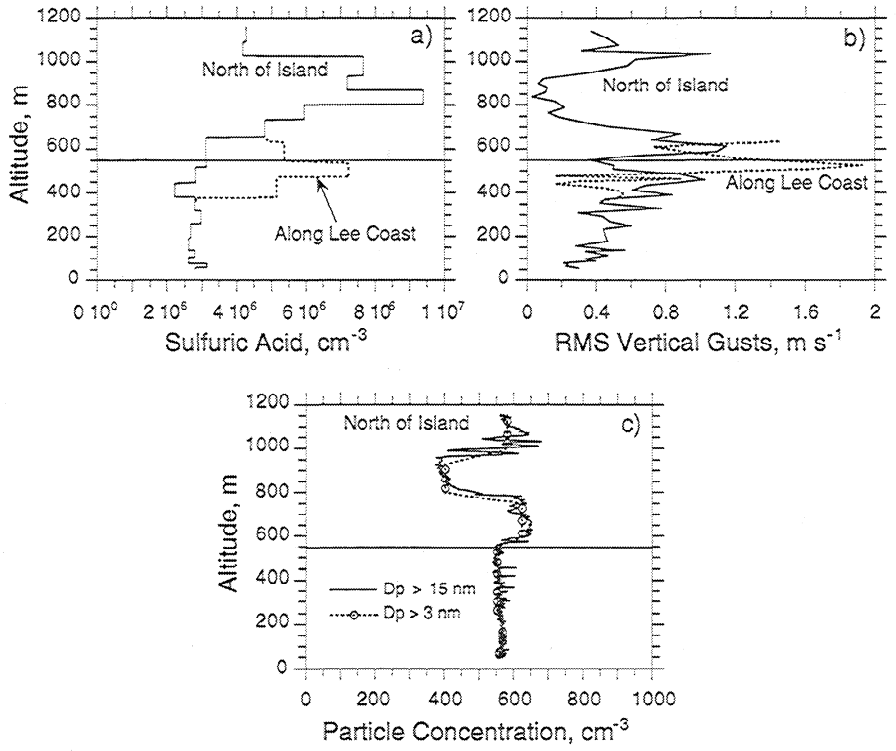

Figure 4. Measurements of (a) $H_2SO_{4(g)}$ concentrations, (b) root-mean-square (rms) of vertical wind gusts in undisturbed air north of the island and along the lee coast (dotted line), and (c) the particle concentrations in undisturbed air.

Owing to active volcanoes in the region, such as Ruapehu, New Zealand, Big Ben, Australia (Heard Island), and Mount Erebus, Antarctica, the precursors of the $H_2SO_{4(g)}$ may have been of volcanic origin. In an earlier flight, at similar latitudes as Macquaried Island and Big Ben (Heard Island), but west of Macquarie Island, we detected thin layers of high $H_2SO_{4(g)}$ concentrations (~10^7 cm^{-3}) just above temperature inversions at altitudes of 2.4 and 3.7 km asl. Layers of high $H_2SO_{4(g)}$ concentrations were not detected in other regions during the ACE 1 campaign. Island-induced mixing of air above the inversion into the boundary layer likely accounts for the elevated $H_2SO_{4(g)}$ concentrations in the upper boundary layer in the island's wake. This mixing is illustrated in Figure 4b which shows elevated rms (root-mean-square) vertical wind velocities in the wake near the inversion.

Finally, Figure 4c shows particle concentrations from both the UCPC (Dp>3 nm) and the NCAR 3760 (Dp>15 nm) in undisturbed air. Particle levels were very uniform in the undisturbed boundary layer, ranging from 550 to 600 cm^{-3}; they then jumped to about 650 cm^{-3} above the inversion and dropped to approximately 400 cm^{-3} in the region of elevated $H_2SO_{4(g)}$ concentrations. The correlation of high $H_2SO_{4(g)}$ concentrations with low particle concentrations may have been from the lack of scavenging of $H_2SO_{4(g)}$ by particles at these altitudes. No evidence of nucleation was ever observed from the aircraft in undisturbed air in the vicinity of the island. For example, the average value of $\tilde{N}$(3-4) for the sounding north of the island was 0.05±0.07 cm^{-3}.

We now focus on the measurements made on the runs immediately offshore of the lee coast. During these two runs the aircraft passed large penguin colonies scattered along the shore. Our interest is observations of new particle formation in these regions where high concentrations of biogenic species are expected.

7. New Particle Formation Off the Lee Coast

We detected significant levels of nanoparticles at various locations along the lee shore of Macquarie Island. Figure 5 shows the flight path of the two passes downwind of the island. The lines show the aircraft trajectories during the 60 s sampling periods for nanoparticles. Aircraft trajectories during consecutive measurements are identified by sample numbers. Thin lines are periods when few or no nanoparticles were recorded, whereas the thick bands are measurements where we recorded high concentrations of nanoparticles (i.e., nanoparticle concentrations greater than 100 cm^{-3}). Figure 5 also shows the locations of the large penguin colonies at the Nuggets, Sandy Bay, Lusitania Bay, and Hurd Point, all situated along the lee coast.

To identify regions of new particle formation, Figure 6 shows $\tilde{N}$(3-4) for the various sample locations identified in Figure 5. High levels of $\tilde{N}$(3-4) identify regions where particle formation was occurring or had recently occurred. Figure 6 shows that we saw evidence of nucleation only in regions downwind of the island. Some of the lower concentrations of $\tilde{N}$(3-4) immediately following a measurement of high $\tilde{N}$(3-4) concentrations (e.g., samples 234, 241 and 243) are likely due, at least to some extent, to residual nanoparticles in the aerosol sampling lines from the previous measurement, an unavoidable result of mixing in sampling lines due to obstacles, such as bends. By far, the

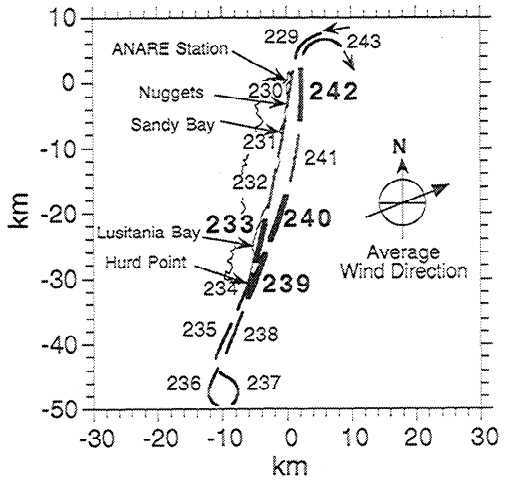

Figure 5. Aircraft measurements along the lee coast of Macquarie Island. Bands indicate aircraft trajectories during the 60 s sample interval to measure nanoparticle concentrations. Consecutive nanoparticle measurements are identified by sample numbers. Locations of the ANARE station and four of the largest penguin colonies on Macquarie Island are also identified by name.

highest concentrations of nanoparticles were detected at sample locations 233, 239, 240, and 242. Comparison with Figure 5 shows that samples 233 and 240 were downwind of the Lusitania Bay colony, 239 the Hurd point colony, and 242 the Nuggets colony, with some possible influence from the Sandy Bay colony. Note that three of the four episodes of high nanoparticle concentrations were detected on the second run which was farther offshore and at higher altitudes than the first run along the coast. (Detailed altitude information is given in Figure 8.)

Sample 242 is also downwind of the ANARE station raising the possibility that the nanoparticles in this case could be of anthropogenic origin. If so, concentrations of larger particles might also be expected to be much higher than background levels. This was not observed. The NCAR 3760 on the aircraft, which measures particles larger than ~15 nm, only recorded concentrations in this region of 486 cm^{-3}, slightly lower than levels in undisturbed air (Figure 4c). The UCPC (Dp > 3 nm) recorded concentrations of 761 cm^{-3}. Thus in terms of particle numbers, the only difference between the downwind sample 242 and undisturbed air was the high levels of nanoparticles emanating from the island. We believe that these particles were formed by nucleation involving biogenic species from the northern penguin colony and not influenced by the ANARE station.

Focusing on the episodes of high nanoparticle concentrations, Figure 7 shows the nanoparticle size distributions for samples 233, 239, 240, and 242. Distributions 233, 239, and 242 are all very similar and show that the nanoparticles detected were all near the lower detection limit of our instrument and suggest that there were large numbers of smaller undetectable particles present. It is likely that these particles were just recently formed by nucleation of gas phase species. However, distribution 240 stands apart, having higher levels of larger-sized nanoparticles. This may be due to a number of factors. First, compared to the other three measurements, 240 was, on average, obtained farther downwind from the island than the other three. This would permit more time for newly formed particles to grow to larger sizes. Second, concentrations of condensable gas phase species may have been higher at this location leading to higher growth rates. Combined with a longer growth time, this would lead to large particles and possibly higher numbers as more previously nucleated particles grow to detectable sizes. Finally, the small structure in the distributions for diameters larger than ~4 nm is likely not real but an artifact of the inversion due to limitations with our present kernel functions [*Weber et al.*, 1997b].

Ground measurements at the ANARE station provided evidence of infrequent high levels of nanoparticles at other times during the period of the ACE 1 study. In these rare cases, the wind direction was from the south, bringing air of island influence. It was only in these cases that evidence of new particle formation was detected at the ground-based site.

To study what species participated in particle formation, Figure 8 shows the time variation of aircraft altitude, rms vertical wind gust velocity, $H_2SO_{4(g)}$ concentration, and $H_2O_{(g)}$ concentration for the measurements along the coast. Sampling intervals corresponding to those shown in Figure 5 are identified

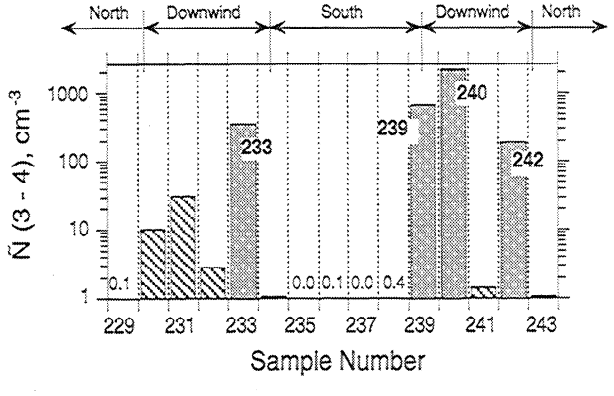

Figure 6. Estimated concentrations of nominally 3 to 4 nm particles measured along the lee coast of Macquarie Island. The high sensitivity of this measurement makes it useful for identifying regions where nanoparticle concentrations are very low, or zero. The figure shows that practically no nanoparticles were detected in undisturbed air and highest concentrations were recorded downwind of penguin colonies (see Figure 5).

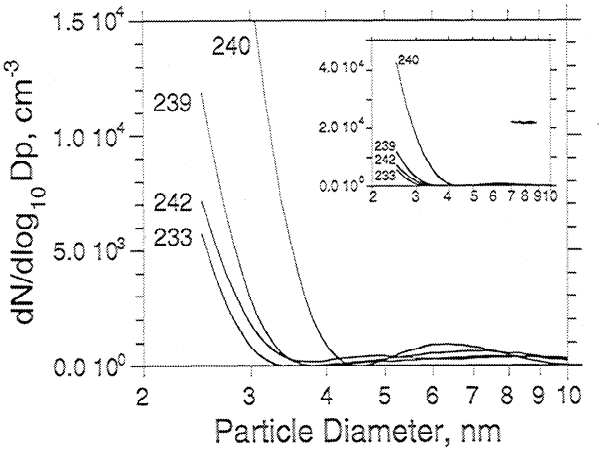

Figure 7. Nanoparticle size distributions recorded immediately downwind of penguin colonies. The distributions are identified by sample numbers. Locations of measurements can be seen in Figure 5. The insert shows the complete distribution for sample 241.

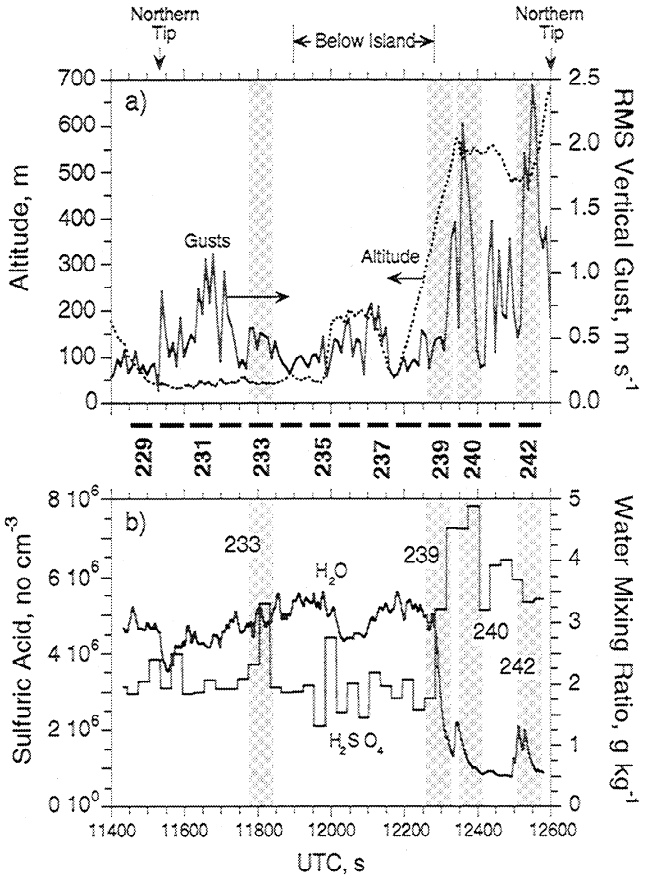

Figure 8. Variation of (a) aircraft altitude and rms vertical wind gusts and (b) $H_2SO_{4(g)}$ concentration and $H_2O_{(g)}$ concentration along the lee shore of Macquarie Island. The dashes below Figure 8a show the periods for each nanoparticle sample. The shaded regions highlight periods of recent large nucleation events.

by the black dashes below Figure 8a, and the four episodes where high nanoparticle concentrations were recorded are shaded. Figure 8a shows that the first pass along the coast was at a low altitude, below 100 m asl. By comparison with Figures 3 and 4, Figure 8b shows that at this altitude, $H_2O_{(g)}$ and $H_2SO_{4(g)}$ concentrations downwind of the island were similar to those of the undisturbed boundary layer. After turning around to the south of the island, the aircraft climbed, reaching an altitude of 400 m asl as it passed the southern tip of the island (during sample 239), and continued climbing as we traveled along the island to about 550 m asl, the height of the inversion in undisturbed air. The aircraft then stayed near this altitude for the remainder of the distance of the downwind leg. As discussed above, this is a region of island-induced turbulent mixing of upper level air, containing high $H_2SO_{4(g)}$ levels, with lower level air, which would contain biogenic species when downwind of the colonies. For example, samples 239, 240, and 242 were all made in regions of enhanced mixing, indicated by the relatively higher value of rms vertical gusts shown in Figure 8a. At these locations, $H_2SO_{4(g)}$ levels were higher (6-7 x 10^6 cm^{-3}) than at similar altitudes in undisturbed air (2 to 3 x 10^6 cm^{-3}). Water vapor, a tracer for surface air, was lower during these samples (0.5 to 1.5 g kg^{-1}) than in the undisturbed boundary layer (2.5 to 3.5 g kg^{-1}) but was higher than above the inversion (0.3 to 0.5 g kg^{-1}). It was in this mixed region, downwind of the penguin colonies, where the highest concentrations of nanoparticles were recorded (see Figure 7).

On the first low-altitude pass, the highest levels of nanoparticles were recorded at sample 233, downwind of the Lusitania Bay colony (Figure 5). However, we did pass the other colonies on this low-altitude run, but significantly fewer nanoparticles were measured in these regions (Figure 6). At these altitudes, concentrations of biogenic species would be very high downwind of colonies. It is interesting to note that the highest levels of nanoparticles observed in the low-altitude pass, sample 233, are correlated with a small localized spike in $H_2SO_{4(g)}$ concentration and the highest $H_2SO_{4(g)}$ concentrations encountered during this run. Figure 9 shows that all the downwind measurements, except for sample 241, show a rough correlation between $\tilde{N}$(3-4) and $H_2SO_{4(g)}$ concentrations. For sample 241, few nanoparticles were formed despite fairly high $H_2SO_{4(g)}$ concentrations. This again points to the role of biogenic species since 241 was not downwind of a large colony (Figure 5).

Calculations of the bimolecular H_2SO_4/H_2O nucleation rate shows that this mechanism is much too slow to account for the high nanoparticle levels recorded downwind of Macquarie Island. Of the sites where high nanoparticle concentrations were observed, the optimal conditions for H_2SO_4/H_2O nucleation were at sample 233 due to the highest relative humidities associated with the lower altitudes (59%). For sample 233, at the ambient temperature of 4.4°C, a $H_2SO_{4(g)}$ concentration of over 10^8 molecules cm^{-3} would be required for a H_2SO_4/H_2O nucleation rate of ~1 particles cm^{-3} s^{-1}. For the observed $H_2SO_{4(g)}$ concentration of 3 x 10^6 molecules cm^{-3}, H_2SO_4/H_2O nucleation would not occur [*Jaecker-Voirol and Mirabel*, 1989].

Although these measurements do not prove our earlier hypothesis that $NH_{3(g)}$ significantly enhances nucleation rates involving $H_2SO_{4(g)}$, the observations are consistent with this hypothesis. Overall, the data show that nanoparticles resulting from recent nucleation were only observed downwind of

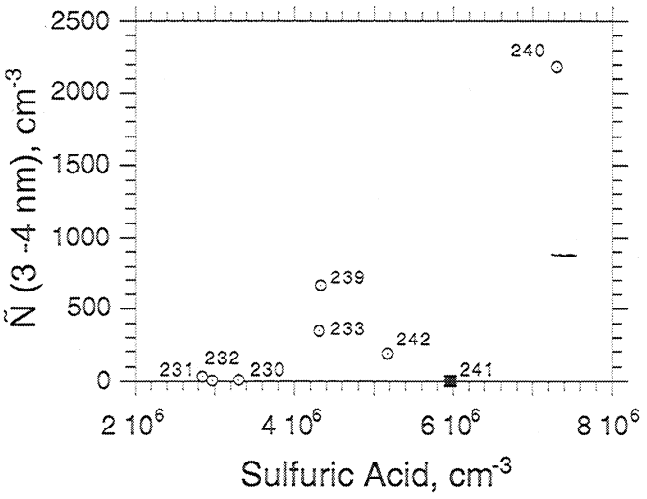

Figure 9. Estimates of nominally 3 to 4 nm particle concentrations versus $H_2SO_{4(g)}$ concentrations recorded immediately downwind of Macquarie Island. Individual measurements are identified by sample numbers, (e.g., see Figure 5). With the exception of sample 241, nanoparticle concentrations were related to $H_2SO_{4(g)}$ concentrations. Sample 241 was in a region of high $H_2SO_{4(g)}$ concentrations but not downwind of penguin colonies.

penguin colonies, and there is evidence that $H_2SO_{4(g)}$ participated in some way. These observations could be due to one or both of two factors. First, nucleation may have been limited by the $H_2SO_{4(g)}$ concentration. Downwind of colonies we would expect biogenic species to be in great excess of $H_2SO_{4(g)}$. Thus, if $H_2SO_{4(g)}$ participated, nucleation rates could be limited by the $H_2SO_{4(g)}$ and higher nanoparticle concentrations would be associated with higher $H_2SO_{4(g)}$ concentrations, consistent with our observations. Alternatively, because it takes a finite amount of time for newly formed particles to grow to a detectable size, if particle growth is limited by $H_2SO_{4(g)}$ uptake (we have assumed this in our previous work), then again, higher nanoparticle concentrations would be associated with higher $H_2SO_{4(g)}$ concentrations. In either case, the measurements strongly suggest that a biogenic species was involved in nucleation. Next, we study the evolution of the newly formed nanoparticles to gain insights into particle growth rates.

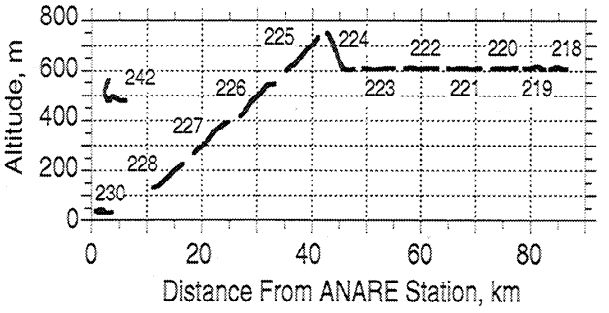

Figure 11. Altitude of nanoparticle measurements made downwind of the northern tip of Macquarie Island. The position of these measurements relative to the island can be seen in Figure 10. The figure is not to scale and greatly exaggerates vertical separation of measurements relative to downwind distance. Sample 229 was not downwind of the island and is not shown.

8. Evolution of the Nanoparticle Spectra Downwind

8.1. Climatology Downwind of the Island

Concentrations of nanoparticles formed near the source of biogenic emissions will change as they are advected away from the island due to processes such as growth, scavenging by larger particles, dilution, and various deposition mechanisms. Some of these effects can be studied by comparing nanoparticle size distributions at various distances downwind from the island. Here, we focus on the growth of newly formed particles.

The only measurements made far downwind of the island were those northeast of the ANARE station made prior to the runs along the lee shore (Figure 1). On the basis of wind direction, only measurements made at the southern end of the higher-altitude circle (609±2 m asl), labeled C in Figure 1, were downwind of the island. These measurements are shown in Figure 10. The other circles, A (39±19 m asl) and B (225±9 m asl), shown in Figure 1, were in the boundary layer and thus in westerly (250±7° from north) flows and were in air that did not pass over the island. This is supported by our aerosol data. We saw essentially no nanoparticles during these low-altitude circles, and total particle concentrations were typical of undisturbed air. However, the final circle on the approach to the island was at an altitude of ~600 m where wind directions had a more southerly component. At this altitude, the wind direction indicates that for the bottom portion of this circle, air would have passed over the northern part of the island.

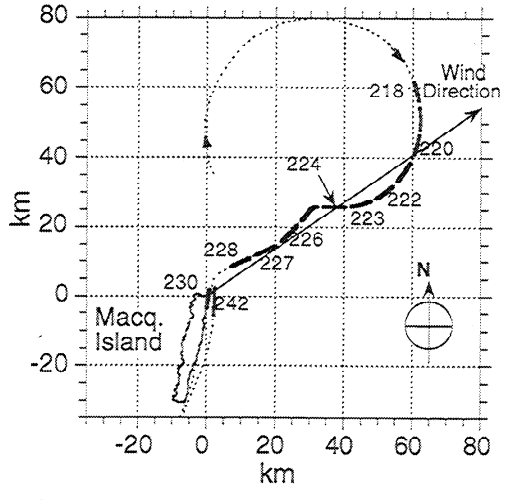

Figure 10. Aircraft flight path and measurements that were downwind of Macquarie Island. Individual nanoparticle measurements are identified by blank bands and sample numbers. The average wind direction of 237° from north for samples 242, 227 and 226 is also shown.

Considering only measurements on the 600 m altitude circle and the descent to the island, Figure 10 shows the location of the various nanoparticle measurements, and Figure 11 shows the altitude of these measurements with respect to distance from the ANARE station. Note that Figure 11 is not to scale and greatly exaggerates the vertical distance between measurements relative to their distance downwind of the island. As before, the lines in Figures 10 and 11 represent the trajectory of the aircraft during each 60 s sample interval and are identified by sample numbers.

Measurements of $H_2O_{(g)}$ concentration showed that the aircraft entered the edge of the island's plume between measurements 217 and 218. These measurements were made at the same altitude (610 m asl), yet the $H_2O_{(g)}$ concentration jumped from 0.54 g kg^{-1} at sample 217 to 1.9 g kg^{-1} for sample 218 and remained at these levels for the following samples. The cause for this increase in $H_2O_{(g)}$ concentration was island-induced mixing which transported water vapor to elevations above the undisturbed air inversion.

The descent to the ANARE station (samples 225 to 230, Figure 11) provided some information on the atmospheric structure far downwind of the island. This sounding gives only a rough idea of the profile since the descent was gradual and covers a horizontal distance of roughly 40 km. Figure 12 shows the temperature, $H_2O_{(g)}$ and $H_2SO_{4(g)}$ concentration profiles in the island's wake along with those for undisturbed air north of the island. These soundings show that the atmosphere in the wake is similar to the undisturbed air in that the temperature inversion, although weaker, is near 550 m asl. Water vapor concentrations were lower above the inversion, while starting at about 700 m asl, $H_2SO_{4(g)}$ concentrations rose sharply with altitude above the inversion. However, there are differences due to island-induced mixing. The boundary layer in the wake is slightly warmer and dryer, and $H_2SO_{4(g)}$ concentrations are

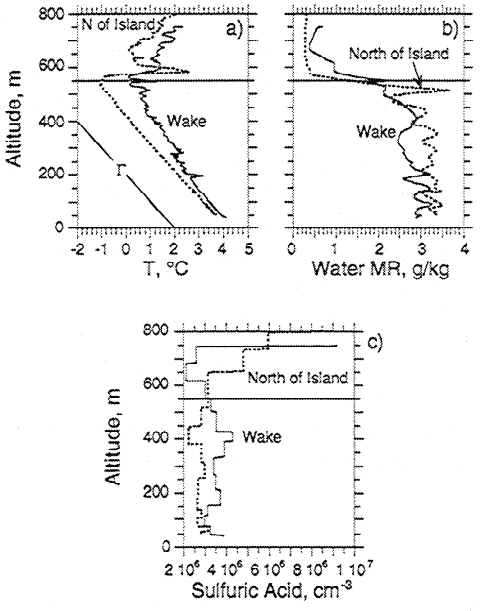

Figure 12. Atmospheric structure in the wake of the island compared to undisturbed air north of the island: (a) temperature, (b) water mixing ratio, and (c) $H_2SO_{4(g)}$ concentration. The temperature inversion, although weaker, still persisted at ~550 m asl. Comparisons show that island-induced mixing resulted in a warmer, dryer boundary layer with slightly higher $H_2SO_{4(g)}$ concentrations than the undisturbed boundary layer.

slightly higher, compared to undisturbed air. For example, the average temperature in the boundary layer in undisturbed air was 1.4°C versus 2.0°C in the wake. Boundary layer $H_2O_{(g)}$ concentrations were 3.1 in undisturbed and 2.7 g kg^{-1} in the wake, and undisturbed $H_2SO_{4(g)}$ concentrations were 2.7 x 10^6 and 3.5 x 10^6 cm^{-3} in the wake.

Mixing also extended the surface influence to higher altitudes with increasing distance from the island. Samples 218 to 223 in Figure 11 were made at an average altitude of 608±4 m asl. In undisturbed air, this altitude is clearly above the inversion, associated with an average $H_2O_{(g)}$ concentration of 0.5 g kg^{-1} (see Figure 12b). From the sounding in the island's wake, at 608 m asl, we were still above the inversion, and the average $H_2O_{(g)}$ concentration was 1.0 g kg^{-1} (also shown in Figure 12b). However, farther downwind in the island's wake (samples 218 to 223), the average $H_2O_{(g)}$ concentration was considerably higher (1.7±0.2 g kg^{-1}). This indicates a boundary layer influence at higher altitudes, but also shows that measurements 218 to roughly 225 were all at an altitude situated right at the transition between the two layers. This complicates the analysis in this region. The significant wind shear at this altitude (e.g., Figure 3d) makes it unclear what trajectory the air masses followed to reach these points, and mixing of nanoparticle-free air from above the inversion will alter nanoparticle concentrations. However, measurements 226 to 230, and 242, all closer to the island, were at altitudes within the boundary layer and thus were minimally influenced by clean upper level air.

With this in mind, Figure 13 shows the changes in nanoparticle (~3 to 10 nm), condensation nuclei (CN) (Dp >15 nm), and $H_2SO_{4(g)}$ concentrations with distance from the ANARE station. In this case, nanoparticle concentrations were determined by integrating over our pulse height-derived nanoparticle distributions for particles between 2.7 and 10 nm. Note, sample 221 is not shown in Figure 13a since in this case the inversion to obtain the nanoparticle distribution failed. In Figure 13a, nanoparticle concentrations are seen to increase with distance from the island, reaching a maximum somewhere in the range of 30 km downwind (e.g., sample 226) and then decrease with distance. CN concentrations only underwent minor changes with downwind distance (Figure 13b). Only at distances of ~45 to 75 km downwind (samples 220 to 224, ignoring 225 which appears to be an anomaly) are CN levels above those of undisturbed air. Figure 13c shows that $H_2SO_{4(g)}$ concentrations tended to decrease slightly with downwind distance.

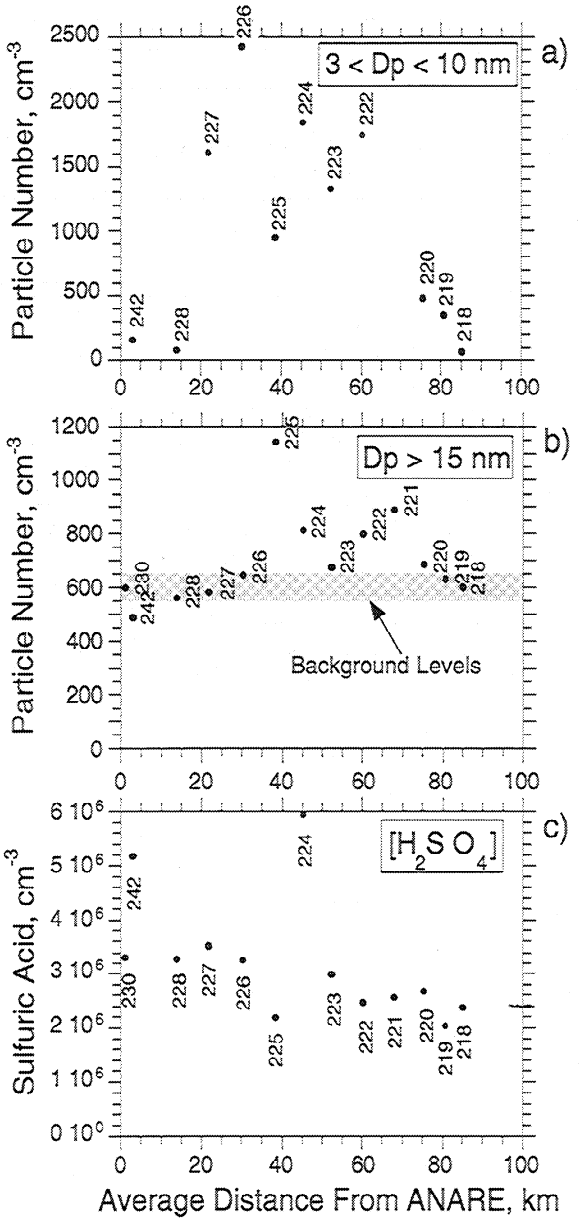

Figure 13. Variation of (a) nanoparticles (~3 to 10 nm diameter), (b) all particles larger than 15 nm (CN), and (c) $H_2SO_{4(g)}$ concentrations with average distance from the ANARE station at the northern tip of Macquarie Island. Nanoparticle concentrations are based on the inversion of UCPC pulse height distributions. Concentrations of particles larger than 15 nm were measured with the NCAR TSI 3760 CPC. Measurements are identified by sample numbers. CN and $H_2SO_{4(g)}$ concentrations are averages over the nanoparticle sample interval (60 s).

The increase in nanoparticle concentrations with increasing downwind distance prior to sample 226 is likely due to growth of the newly formed particles into our measurement size range (Dp>2.7 nm). The decrease in concentration with distance after 226 could be a combination of growth out of the nanoparticle range, loss through scavenging by larger particles, and dilution by mixing with upper level air containing no nanoparticles. Mixing appears to be the most likely cause for the decrease. The sudden drop in nanoparticle levels for samples 218 to 220 may be due to the close proximity to the inversion. Note that the corresponding CN levels (218 to 220) also dropped to background concentrations. The observation of high nanoparticle and CN for samples 221 to 225, all of which are near or above the inversion, is difficult to explain. The high levels may be due to the fact that wind directions associated with these altitudes suggest that the air reaching these points was more from the middle of the island, regions where we observed higher nanoparticle concentrations when sampling just offshore. Finally, the CN data close to the island show no evidence of enhanced levels due to new particle formation. This indicates that the newly formed nanoparticles, shown in Figure 13a, were less than 15 nm diameter.

Nanoparticle size distributions for samples 242, 227, 226, 224, 223, and 220 are shown in Figure 14. The other distributions not plotted were similar in shape to those of Figure 14. The distributions show the results of the processes discussed above. Close to the island there is evidence of recent or ongoing nucleation followed by growth of the newly formed particles. Samples 242 and 227 show high levels of nanoparticles smaller than 3 nm, and with respect to sample 242, distributions 227 and 226 progressively shift to larger sizes with increasing downwind distance. Growth may also account for the increase in the smallest particles of sample 227 compared to 242, as more of the newly formed particles reach the instrument lower detection limit. Whereas, by sample 226, the newly formed particles appear to have grown past the detection limit resulting in a reduction of the concentration of smallest sizes. After sample 226 (except for sample 222, which is not plotted), the distributions show little evidence of growth. The primary change was a reduction in nanoparticles with increasing distance. Preferential scavenging of the more mobile smaller particles in these distributions (and not growth) can explain the shift in the peaks of these distributions to larger sizes. The lack of growth for these farther offshore nanoparticles may be a result of a differing climatology than those particles measured closer to the island, due to their proximity to the inversion.

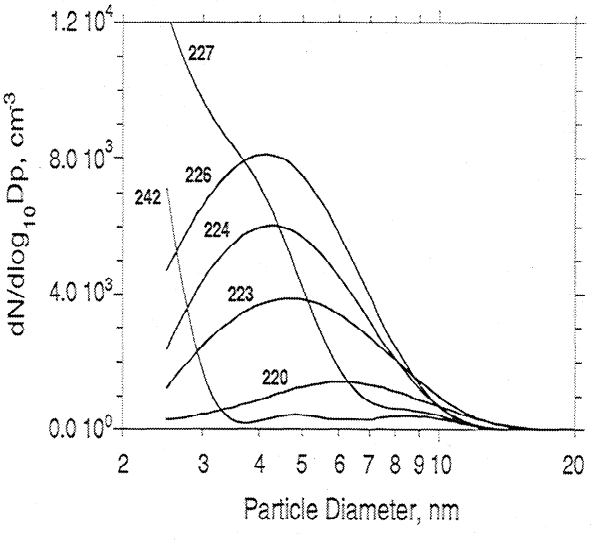

Figure 14. Selected nanoparticle size distributions measured far downwind of Macquarie Island. Locations of measurements can be seen in Figure 10. The sequence of measurements with increasing downwind distance is 242, 227, 226, 224, 223, and 220. The distributions show growth of newly formed particles to larger sizes close to the island and then depletion of nanoparticles with increasing downwind distance.

Using the wind speed to estimate the time for transport of particles between measurement locations, the observed changes in nanoparticle distributions close to the island are now used to estimate average nanoparticle growth rates. These observed growth rates are then compared to the predicted growth rate if only $H_2SO_{4(g)}$ and associated H_2O condensed onto the newly formed particles.

8.2. Nanoparticle Growth Rates

The size distribution at sample 242 in Figure 14 indicates that most nanoparticles were smaller than approximately 3 nm. By measurement 227, however, there were significant numbers of nanoparticles up to about 5.5 nm, and by measurement 226, particles had grown to about 8 nm. The time for this growth can be estimated from the average position between measurements and the average wind speed, assuming no lateral mixing of air having different nanoparticle characteristics occurred during this time. We also ignore coagulation as a mechanism of nanoparticle growth since it is insignificant for these concentrations and timescales. The distance between measurements was calculated along the line of average wind direction which for these measurements was 237±6 ° from north, as shown in Figure 10. The uncertainty in the distance between measurements was taken as half the distance the aircraft traveled in a 60 s sample (e.g., ~3 km). The average wind speed, based on measurements 226, 227, and 242, was 6.4±1.1 m s^{-1}. The first two rows in Table 2 summarize the observations used to estimate the nanoparticle growth rates from these distributions. These calculations suggest that average nanoparticle growth rates were in the range of 2 to 5 nm h^{-1}.

Table 2. Measurements Used to Estimate Growth Rates of Nanoparticles

Measurement Numbers	Distance, km	Time, hours	Change in Diameter, nm	Estimated Growth Rate, nm h^{-1}
242 to 227	20±3	0.87±0.23	from 3 to 5.5	3±1
242 to 226	28±3	1.22±0.20	from 3 to 8	4±1
Island to 227	27±3	1.17±0.24	from 1 to 5.5	4±1
Island to 226	38±3	1.65±0.31	from 1 to 8	4±1

The first two rows show estimates based on the observed changes in nanoparticle distributions 227 and 226 with respect to distribution 242. The last two rows show estimated growth rates based on times for vapor, on the lee side of the island, to reach maximum sizes observed in the indicated measurement. The average wind speed was 6.4±1.1 m s^{-1}. The relative positions of these measurements are shown in Figures 10 and 11, and the distributions are plotted in Figure 14. The uncertainty in the change in diameter was assumed to be ±1 nm.

If growth is limited by the rate of uptake of $H_2SO_{4(g)}$, the maximum expected nanoparticle growth rate would be

$$\frac{dD_p}{dt} \approx \alpha_{H_2SO_4} \nu_1 \frac{[H_2SO_4]}{2} \bar{c} \quad (1)$$

where $\bar{c}$ is the average thermal speed of the condensing vapor species and ν_1 is the volume gained by the addition of a H_2SO_4 molecule. This volume includes species that would also be adsorbed after the addition of the H_2SO_4 to maintain phase equilibrium, such as H_2O and possibly NH_3. In this case, we only consider H_2O and estimate ν_1 from bulk solution properties. Ammonia is not considered due to the lack of thermodynamic solution data for the $H_2SO_4/NH_3/H_2O$ system. However, if $NH_{3(g)}$ participates by neutralizing the H_2SO_4 aerosol, forming ammonium sulfate ($(NH_4)_2SO_4$) particles, the growth rate will be similar to that of H_2SO_4 since the molecular volume and the degree of hydration are similar for H_2SO_4 and $(NH_4)_2SO_4$ aerosols [*Nemesure et al.*, 1995]. We also assume an accommodation coefficient ($\alpha_{H_2SO_4}$) of 1 [*Jefferson et al.*, 1997] and ignore reevaporation of H_2SO_4.

The average $H_2SO_{4(g)}$ concentration for samples 242, 227, and 226 was $3.8 \times 10^6 \pm 0.8 \times 10^6$ molecules cm^{-3}, and the average temperature and relative humidity were 1.7 ± 0.9 °C and 45 ± 9%, respectively. Using these values, equation (1) gives an average growth rate by condensing H_2SO_4-$(H_2O)_n$ of 0.4 ± 0.1 nm h^{-1}. The uncertainty is due primarily to the uncertainty in $H_2SO_{4(g)}$ concentrations, assumed to be 30%. Thus the observed nanoparticle growth rates are difficult to explain by $H_2SO_{4(g)}$ condensation since the observed growth were from roughly 4 to 17 times higher. This is similar to our findings at the remote continental site in Colorado where we observed growth rates higher by factors of ~5 to 10 [*Weber et al.*, 1997a]. It is highly unlikely that this difference can be explained by our underestimating the H_2SO_4 concentration since to achieve the observed growth, $H_2SO_{4(g)}$ concentrations would need to be higher by similar factors (e.g., $H_2SO_{4(g)}$ concentrations ranging from $\sim 2 \times 10^7$ to 7×10^7 molecules cm^{-3}). Our measurements in the vicinity of Macquarie Island show no evidence that $H_2SO_{4(g)}$ concentrations reached these levels.

Our estimates of observed growth rates have been based on changes in nanoparticle size distributions measured at different locations. This assumes that one distribution evolved from the other. This may not be true, since these measurements were made at different altitudes, and we did observe wind shear in the boundary layer. Moreover, dispersion of the aerosol plume would also complicate the analysis. This analysis becomes more tenuous when comparing distributions that are farther apart. An alternative approach for estimating growth rates that does not assume evolution of a single nanoparticle distribution is to assume the island is the starting point for growth of a vapor molecule. Observed growth rates can then be estimated from the transport time from the coast to the location of the measurement. From nanoparticle distributions 227, and 226, particles reached maximum diameters of roughly 5.5 and 8 nm, respectively (see Figure 14). The corresponding distances from the Sandy Bay colony to these positions were, roughly, 27 and 38 km, respectively. Note that this is a conservative estimate since this distance is longer than the closest straight line distance to the island. Thus, if particles were formed at some other location, closer to the ANARE station, the distance would be shorter, and we will have underestimated the observed growth rates. On the basis of an average wind speed of 6.4 m s^{-1}, and assuming a vapor molecule is approximately 1 nm in diameter, the observed growth rates from samples 227 and 226 were roughly 4 nm h^{-1}. These results are summarized in the last two rows of Table 2. These findings are consistent with our previous calculation of observed growth rates.

Growth rates of the order of a few nanometers per hour are also consistent with our observations of much higher nanoparticle concentrations on the second versus on the first leg along the lee coast. For the first pass, we were typically ~1 km downwind, while on the second traverse, we were ~3 to 4 km downwind (see Figure 5). At an average wind speed of 7 m s^{-1}, average growth rates of ~40 nm h^{-1} would be required to grow particles to our detection limit of ~2.7 nm in a distance of 1 km. However, growth rates of ~10 nm h^{-1}, similar to the values calculated above, would be sufficient to grow particles to detectable sizes for the offshore distances on the second pass.

Although our estimates of the nanoparticle growth rates are approximate, they consistently give growth rates of newly formed particles of the order of 1 to 10 nm h^{-1}, about a factor of 4 to 17 times higher than growth by condensing $H_2SO_{4(g)}$ and associated H_2O. At Macquarie Island, it is unclear what causes the enhanced growth. Similar findings in the Colorado study were attributed to organic species associated with forested regions [*Marti et al.*, 1997b; *Weber et al.*, 1997a]. These species would not have been present in this location. Fast growth may have been from other biogenic species associated with the colonies which we have not considered. Organic gases associated with seawater and decaying coastal vegetation may also have been present due to the action of waves breaking along the island coast. It is also possible that these discrepancies in growth rates arise from a limited understanding of the microphysics of this process.

Finally, the observed decrease in nanoparticle concentrations for samples 224, 223, and 220 (Figure 14) cannot be entirely accounted for by scavenging. These measurements made far from the island were all situated at the inversion, and therefore the observed depletion could also be due to entrainment of particle free air during advection away from the island.

9. Conclusions

Measurements in the vicinity of Macquarie Island during ACE 1 provided a unique opportunity to study, in situ, the role of biogenic species on the formation and growth of newly formed particles. Nanoparticle distributions measured by UCPC pulse height analysis showed high concentrations of nanoparticles near the instrument lower detection limit (~2.7 nm) only when downwind of large penguin colonies, presumably corresponding to regions of high concentrations of species of biogenic origin. Highest nanoparticle concentrations were found downwind of colonies in regions of enhanced mixing of upper level air containing elevated $H_2SO_{4(g)}$ concentrations. The data strongly suggest that a biogenic species was involved in particle formation and that $H_2SO_{4(g)}$ may have also participated. The results are consistent with the hypothesis that $H_2SO_4/NH_3/H_2O$ nucleation rates are significantly higher than bimolecular H_2SO_4/H_2O nucleation. However, it is still unknown whether these species nucleate by themselves or if other species, possibly including ions, also participate.

Observations of the evolution of nanoparticle distributions to larger sizes during advection away from the island showed clear

evidence of growth of the newly formed particles. From these measurements, we estimated that the nanoparticles grew at rates ranging from roughly 2 to 5 nm h^{-1}, about a factor of 4 to 17 times higher than growth by condensing $H_2SO_{4(g)}$ and associated H_2O. These rates are similar to our observations of nanoparticle growth at a clean continental site, where we speculated that enhanced growth was due to naturally occurring species, such as oxidized terpenes. It is unclear what accounts for the fast growth rates observed in this study. Future work will examine the role of $NH_{3(g)}$ using currently unavailable data.

Acknowledgments. We thank the National Center for Atmospheric Research (NCAR) Research Aviation Facilities (RAF) for the use of their data. The National Center for Atmospheric Research is sponsored by the National Science Foundation. This research is a contribution to the International Global Atmospheric Chemistry (IGAC) Core Project of the International Geosphere-Biosphere Program (IGBP) and is part of the IGAC Aerosol Characterization Experiments (ACE). This research was supported by NASA through grant NAGW-3767. Research at BNL was performed under the auspices of the U.S. Department of Energy contract DE-AC02-76CH00016 Atmospheric Chemistry Program within the Office of Health and Environmental Research.

References

Bates, T. S., V. N. Kapustin, P. K. Quinn, D. S. Covert, D. J. Coffman, C. Mari, P. A. Durkee, W. J. DeBruyn, and E. S. Saltzman, Processes controlling the distribution of aerosol particles in the lower, marine boundary layer during ACE 1, *J. Geophys. Res.*, this issue (a).

Bates, T. S., B. J. Huebert, J. L. Gras, F. B. Griffiths, and P. A. Durkee, The International Global Atmospheric Chemistry (IGAC) Project's First Aerosol Characterization Experiment (ACE 1): Overview, *J. Geophys. Res.*, this issue (b).

Brechtel, F. J., S. M. Kreidenweis, and H. B. Swan, Air mass characteristics, aerosol particle number concentrations, and number size distributions at Macquarie Island during ACE 1, this issue.

Charlson, R. J., J. E. Lovelock, M. O. Andreae, and S. G. Warren, Oceanic phytoplankton, atmospheric sulfur, cloud albedo and climate, *Nature*, *326*, 655-661, 1987.

Clarke, A. D., J. L. Varner, F. Eisele, L. Mauldin, D. Tanner and M. Litchy, Particle production in the remote marine atmosphere: Cloud outflow and subsidence during ACE 1, *J. Geophys. Res.*, this issue.

Easter, R. C., and L. K. Peters, Binary homogeneous nucleation: Temperature and relative humidity fluctuations, non-linearity, and aspects of new particle production in the atmosphere, *J. Appl. Meteorol.*, *33*, 775-784, 1994.

Eisele, F. L., and D. J. Tanner, Measurement of the gas phase concentrations of H_2SO_4 and methane sulfonic acid and estimates of H_2SO_4 production and loss in the atmosphere, *J. Geophys. Res.*, *98*, 9001-9010, 1993.

Hegg, D. A., L. F. Radke, and P. V. Hobbs, Particle production associated with marine clouds, *J. Geophy. Res.*, *95*, 13,917-13,926, 1990.

Hegg, D. A., D. S. Covert, and V. N. Kapustin, Modeling a case of particle nucleation in the marine boundary layer, *J. Geophys. Res.*, *97*, 9851-9857, 1992.

Huntzicker, J. J., R. A. Caryke, and C. S. Ling, Neutralization of sulfuric acid aerosol by ammonia, *Environ. Sci. Technol.*, *14*, 819-824, 1980.

Jaecker-Voirol, A., and P. Mirabel, Heteromolecular nucleation in the sulfuric acid-water system, *Atmos. Environ.*, *23*, 2053-2057, 1989.

Jefferson, A., F. L. Eisele, P. J. Ziemann, J. J. Marti, R. J. Weber, and P. H. McMurry, Measurements of the H_2SO_4 mass accommodation coefficient onto polydisperse aerosol, *J. Geophys. Res.*, *102*, 19,021-19,028, 1997.

Kerminen, V., A. Wexler, and S. Potukuchi, Growth of freshly nucleated particles in the troposphere: Roles of NH_3, H_2SO_4, HNO_3, and HCl, *J. Geophys. Res.*, *102*, 3715-3724, 1997.

Kreidenweis, S. M., J. E. Penner, F. Yin, and J. H. Seinfeld, The effects of dimethylsulfide upon marine aerosol concentrations, *Atmos. Environ.*, Part A, *25*, 2501-2511, 1991.

Lin, X., W. L. Chameides, C. S. Kiang, A. W. Stelson, and H. Berresheim, A model study of the formation of cloud condensation nuclei in remote marine areas, *J. Geophys. Res.*, *97*, 18,161-18,171, 1992.

Lindeboom, H. J., The nitrogen pathway in a penguin rookery, *Ecology*, 65, 269-277, 1984.

Marti, J. J., A. Jefferson, X. P. Cai, C. Richert, P. H. McMurry, and F. Eisele, H_2SO_4 vapor pressure of sulfuric acid and ammonium sulfate solutions, *J. Geophys. Res.*, *102*, 3725-3735, 1997a.

Marti, J. J., R. J. Weber, P. H. McMurry, F. L. Eisele, D. J. Tanner, and A. Jefferson, New particle formation at a remote continental site: Assessing the contributions of SO_2 and organic precursors, *J. Geophys. Res.*, *102*, 6331-6339, 1997b.

McMurry, P. H., H. Takano, and G. R. Anderson, Study of the ammonia (gas)-sulfuric acid (aerosol) reaction rate, *Environ. Sci. Technol.*, *17*, 347-352, 1983.

Mizutani, H., and E. Wada, Nitrogen and carbon isotope ratios in seabird rookeries and their ecological implications, *Ecology*, *69*, 340-349, 1988.

Nemesure, S., R. Wagener, and S. E. Schwartz, Direct shortwave forcing of climate by the anthropogenic sulfate aerosol: Sensitivity to particle size, composition, and relative humidity, *J. Geophys. Res.*, *100*, 26,105-26,116, 1995.

Perry, K. D., and P. V. Hobbs, Further evidence for particle nucleation in clear air adjacent to marine cumulus clouds, *J. Geophys. Res.*, *99*, 22,803-22,818, 1994.

Raes, F., Entrainment of free tropospheric aerosols as a regulating mechanism for cloud condensation nuclei in the remote marine boundary layer, *J. Geophys. Res.*, *100*, 2893-2903, 1995.

Raes, F., A. Saltelli, and R. Van Dingenen, Modelling formation and growth of H_2SO_4-H_2O aerosols: Uncertainty analysis and experimental evaluation, *J. Aerosol Sci*, *23*, 759-771, 1992.

Russell, L. M., S. N. Pandis, and J. H. Seinfeld, Aerosol production and particle growth in the marine boundary layer, *J. Geophys. Res.*, *99*, 20,989-21,003, 1994.

Selkirk, P. M., R. D. Seppelt, and D. R. Selkirk, *Subantarctic Macquarie Island*, Cambridge Univ. Press, New York, 1990.

Stolzenburg, M. R., and P. H. McMurry, An ultrafine aerosol condensation nucleus counter, *Aerosol Sci. Technol.*, *14*, 48-65, 1991.

Tyndall, J., On a new series of chemical reactions produced by light, *Proc. R. Soc. London*, *17*, 92-102, 1868.

Weber, R. J., P. H. McMurry, F. L. Eisele, and D. J. Tanner, Measurement of expected nucleation precursor species and 3 to 500 nm diameter particles at Mauna Loa Observatory, Hawaii, *J. Atmos. Sci.*, *52*, 2242-2257, 1995.

Weber, R. J., J. J. Marti, P. H. McMurry, F. L. Eisele, D. J. Tanner, and A. Jefferson, Measured atmospheric new particle formation rates: Implications for nucleation mechanisms, *Chem. Eng. Commun*, *151*, 53-64, 1996.

Weber, R. J., J. J. Marti, P. H. McMurry, F. L. Eisele, D. J. Tanner, and A. Jefferson, Measurements of new particle formation and ultrafine particle growth rates at a clean continental site, *J. Geophys. Res.*, *102*, 4375-4385, 1997a.

Weber, R. J., M. Stolzenburg, S. Pandis, and P. H. McMurry, Inversion of UCNC pulse height distributions to obtain ultrafine (~3 to 10 nm) particle size distributions, *J. Aerosol Sci.*, submitted, 1997b.

Went, F. W., Blue hazes in the atmosphere, *Nature*, *187*, 641-643, 1960.

Went, F. W., On the nature of Aitken condensation nuclei, *Tellus*, *18*, 549-555, 1966.

Wolfenbarger, J. K., and J. Seinfeld, Inversion of aerosol size distribution data, *J. Aerosol Sci.*, *21*, 227-247, 1990.

D. Baumgardner, G. L. Kok, and R. D. Schillawski, Research Aviation Facility, National Center for Atmospheric Research, Boulder, CO 80307. (email: darrel@ncar.ucar.edu; kok@ncar.ucar.edu; rschill@ucar.edu).

F. J. Brechtel and S. M. Kreidenweis, Department of Atmospheric Science, Colorado State University, Fort Collins, CO 80521. (email: fredb@aerosol.atmos.colostate.edu; soniak@aerosol.atmos.colostate.edu).

F. L. Eisele, L. Mauldin, and D. J. Tanner, Atmospheric Chemistry Division, National Center for Atmospheric Research, Boulder, CO 80307. (email: eisele@ncar.ucar.edu; mauldin@acd.ucar.edu; tanner@ncar.ucar.edu).

P. H. McMurry, Particle Technology Laboratory, Department of Mechanical Engineering, University of Minnesota, Minneapolis, MN 55455. (email: mcmurry@me.umn.edu).

R. J. Weber, Environmental Chemistry Division, Brookhaven National Laboratory, Upton, NY 11973-5000. (email: rweber@bnl.gov).

(Received May 30, 1997; revised August 19, 1997; accepted August 27, 1997.)